Improved hybrid DTC technology for eCAR 4-wheels drive

Njock Batake Emmanuel Eric, Nyobe Yome Jean Maurice, Ngoma Jean Pierre, Ndoumbé Matéké Max
Laboratory of Electronics, Electrical Engineering, Automation and Telecommunications (LEEAT),
National Higher Polytechnic School of Douala, University of Douala, Douala, Cameroon

Article Info	ABSTRACT
	This article deals with the design of a hybrid controller (HyC). It combines fuzzy logic (FL), adaptive neuro-fuzzy inference system (ANFIS). It is combined with direct torque control (DTC). This HyC-DTC combination is designed to improve the technical performance of a 04-wheel drive electric vehicle (EV). A stress test is identically applied to the DTC combined with the FL (FDTC) and to the HyC-DTC in order to certify the suitability of this new control following a cross-validation. This is based on dynamic stability criteria (overshoot, rise time, accuracy), analysis of torque and flux oscillations, and the EV's robustness symbol. The EV's magnetic quantities are managed by a master-slave module (VMSC). Simulations are carried out using MATLAB/Simulink software. The HyC-DTC achieves near-zero accuracy like the FDTC, with overshoot around 0.2% less than the FDTC, and torque oscillation amplitude around 4 times less than the FDTC. However, its rise time is 0.045% greater than that of the FDTC. It is therefore slower, but more precise and suitable for EV transmission systems in terms of safety and comfort.

Corresponding Author:

Njock Batake Emmanuel Eric
Laboratory of Electronics, Electrical Engineering, Automation and Telecommunications (LEEAT)
National Higher Polytechnic School of Douala, University of Douala
Douala, Cameroon
Email: e.njockbatake@gmail.com

1. INTRODUCTION

Environmental pollution and the energy crisis are now two focal points that are culminating and constantly expanding. Electric vehicles (EVs), which are propulsion systems whose actuators are mainly electric motors (induction motor, synchronous and variable reluctance motor, direct current machine) [1], are a genuine means of recourse that forms part of the measures taken by the automotive industry to combat these threats. Thanks to their high efficiency and virtually non-existent air and noise pollution, they stand out from other means of transport and are gaining in popularity [2]. There are 4 main categories of electric vehicles: hybrid electric vehicles (HEVs), plug-in electric vehicles (PEVs), fuel cell electric vehicles (FCEVs), and battery electric vehicles (BEVs). They are all subject to the same technical and economic constraints, i.e., design and fuel costs, difficult access to electric charging stations, and battery charging times. The most commercially available EVs are FCEVs and BEVs [3]. There are also four typical motor configurations in an EV: single, dual, triple, and four motors. The first is not suitable for high-power EVs, while dual and triple are less economical and do not offer a satisfactory transmission ratio between the motor and the wheel. The four motor configuration, on the other hand, does not suffer from any of these vagaries, but also has an alternating torque for each motor linked to its wheel. This gives the EV good stability, a wide speed range, and high efficiency [3].

During the design of an EV, the choice of the characteristics of its actuators is a key issue because it is linked to its performance. The induction machine (IM) has technical and economic characteristics that are popular in the automotive industry [4], [5]. However, it cannot function optimally without appropriate control. That is why the direct torque control (DTC) algorithm was developed for her. This algorithm allows control of a three-phase inverter connected directly to the IM for the traction of the EV. It poses a problem, that of the wide range of electromagnetic torque ripple, large currents of harmonic distortions and the variation of the switching frequency [2].

Artificial intelligence during these previous years is considerably implemented in the field of actuator control of EVs. It is continuously valued for its significant impact in improving the energy management of an EV. It is then that in [6] she intervenes in the indirect field control (IFOC) following the introduction of two neuro-fuzzy controllers. The EV presented here has a two-wheel drive configuration. An electronic differential, which takes into account the road profile, allows to control effectively the torque and speeds of the two driving wheels independently in order to obtain satisfactory performance. However, the implementation of this masterpiece requires algorithmic and architectural complexities related to actuator parameters, which can affect the stability of the EV. Houacine *et al.* [7] provide an element of solution to this problem; a carefully profiled method involves fuzzy logic in adaptive momentum and compensation. This increases the maneuverability and stability of the EV under various constraints. The finite control set direct torque control (FDTC) and space vector modulation-direct torque control (SVM-DTC) controls for a twin-engine vehicle are performed and then compared in terms of performance [8]. The results in terms of speed, robustness, and energy savings put the FDTC in pole position compared to the SVM-DTC control. However, the supply of each engine by a converter is quite expensive and increases the size of the traction system.

In the same vein, many systems have been developed with several machines that are powered by a single converter this to significantly reduce the size and cost of the system. Thus, in [9], a brief presentation of the longitudinal control by acceleration slip control and anti-lock braking system is presented. It is based on the DTC combined with a non-linear predictive system for a multi-machine system. This combination leads to advanced control for EVs. The fuzzy logic allows the values of the in-line weighting factors to be determined and the optimal switching states to be generated, optimizing the EV drives precisely. The major drawback is the complexity of the control system illustrated. The [10], a control based on the conventional DTC, is developed for the control of 04 PMSM-type engines for one EV. Here, there are 02 three-phase inverters, so each feeds two engines on either side of the vehicle. This includes a master-slave control module. This module switches between machines and uses an adaptive model reference system for speeds. It is remarkably efficient, although it allows for strong oscillations of torque and stator flow.

In addition, Max *et al.* [10] performed a comparison between the FDTC, the DTC combined with artificial neural networks (DTC-ANNs), and the conventional DTC is performed for a 4-wheel drive to 2-inverter multi-machine architecture, each feeding two wheels located on the same side. The first two strategies are used to adjust the accuracy error on electromagnetic flux and torque, and reduce the amplitude of oscillations in the system emitted by conventional DTC. After investigation, it appears in this case that the FDTC provides better results than the other two techniques used in terms of EV performance. The problem that remains is a considerable and visible amplitude of torque oscillations in the presentation of simulation graphs.

Further, many hybrid controllers have been created by combining various algorithms to improve DTC control of IM. This is the case of the fuzzy controller to improve motor's efficiency [11], [12], the development of several fuzzy controllers [13], and the fusion of sliding mode controllers with FL to perfect the performances of IMs is examined in [14]. The present study proposes the design of a hybrid controller for a HyC-DTC strategy. this FDTC-inspired controller is, in turn, integrated into an EV architecture identical to that of the FDTC [8] with a view to observing the reaction of the whole because and then cross-validating the two technologies to highlight the relevance of the news on the dynamic system performance. This comparison allows not only to validate the proposed hybrid controller, but also to highlight the limits and the added value for the traction chain of a 4-wheel multi-machine system of EVs. The two controllers are each in turn in the same architecture, associated with a VMSC module. This module facilitates the proper management of magnetic actuator quantities (IM) and has been developed in [8]. It should also be noted that the design of the hybrid controller is done in order to provide an effective response to the difficulties caused by a considerable magnitude of the ripples of the characteristic sizes of EV engines (magnetic flux, torque), and their dynamic parameters (overshoot, rising time, steady state error) the previous method [10]. The two methods discussed above differ from the previous classic DTC in the use of control and management mechanisms, such as the PI regulator for speed control and an electronic differential (ED). These mechanisms allow for greater flexibility, responsiveness, precision, and simplicity of implementation. The overall performances are satisfactory, and although the hybrid controller provides a slightly longer response time than the FDTC, he is indeed practiced in using traction on multi-machine systems.

2. ARCHITECTURAL SCHEME AND MODELLING OF THE EV DYNAMICS

2.1. Description of the architecture

The diagram below of Figure 1 shows an EV with four-wheel drive. It consists of speed converters, flux estimators, three-phase to two-phase (3 to 2) transformation modules, two controllers (hybrid or fuzzy logic), each of which in turn feeds an inverter that produces the voltages required (Sa, Sb, Sc) for the rotation of two motors located on the same side, while avoiding them operating in saturation mode. The ED generates the speed profile according to the steering angles. Two VMSC modules feed the FL (respectively HyC) controller which has as inputs the errors of electromagnetic torques, fluxes, and angles produced respectively by each of the lateral actuators (IM), whose outputs are flux and angle values managed by the hybrid controller or the fuzzy controller to produce adequate outputs for the operation of the inverters.
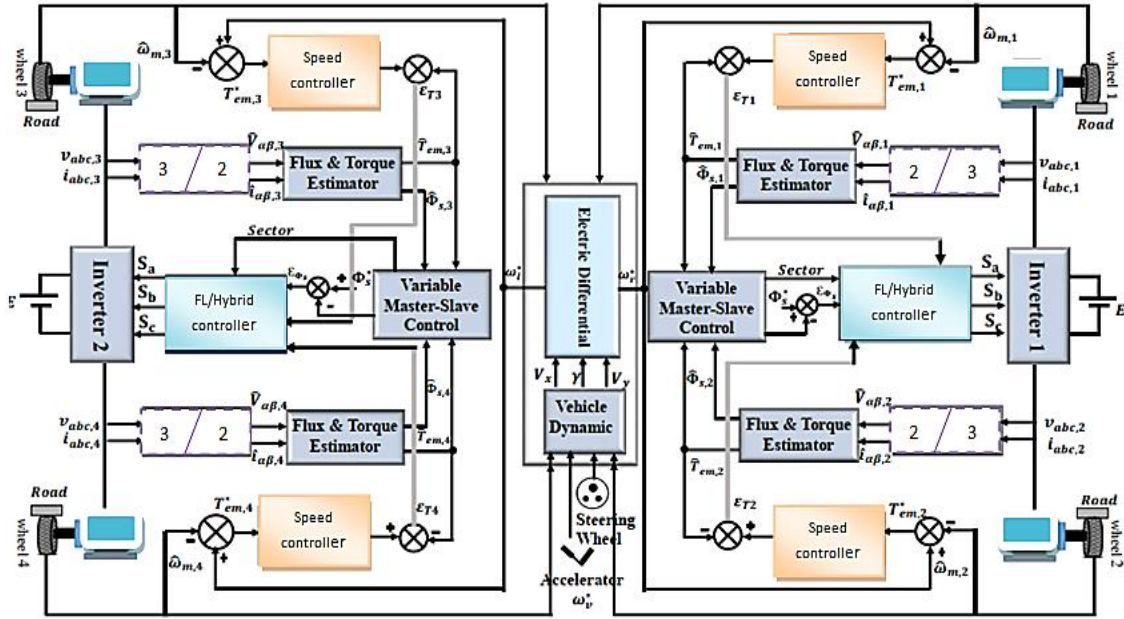

Figure 1. Architectural synoptic diagram of the electric vehicle

2.2. Description of the EV dynamics

The parameters that explicitly describe the vehicle dynamics are the lateral and longitudinal velocities and the radius of curvature [15], [16]. Their expressions are as (1)-(3).

$$v_x = v_y + \frac{F_{t1}+F_{t2}+F_{t3}+F_{t4}-F_{tot}}{M_v} + \frac{C_f*\delta}{M_v}*\left(\frac{v_y+r*l_r}{v_y}-\delta\right) \tag{1}$$

$$v_y = \left(-\frac{C_f+C_r}{M_v*v_x}\right)*v_y + \left(\frac{C_f*l_f+C_r*l_r}{M_v*v_x}-v_x\right)*r + \frac{C_f*\delta}{M_v} \tag{2}$$

$$r = \left(\frac{C_r*l_r-C_f*l_f}{j_v*v_x}\right)*v_y - \left(\frac{C_r*l_r^2-C_f*l_f^2}{j_v*v_x}\right)*r + \frac{C_f l_f*\delta}{j_v} + \frac{d}{j_v}(F_{t1}+F_{t2}+F_{t3}+F_{t4}) \tag{3}$$

During its movement, the vehicle is subject to forces [17]-[19] and stresses, as shown in Figure 2.

$$\text{Tire rolling resistance: } F_{rr} = g * M_v * C_{rr} * \cos(\alpha) \tag{4}$$

$$\text{Aerodynamic resistance in drag: } F_{wind} = 0.5 * \rho * S_f * C_{px} * (V_h - V_{air})^2 \tag{5}$$

$$\text{Levelling resistance: } F_g = g * M_v * \sin(\alpha) \tag{6}$$

$$\text{Acceleration resistance: } F_l = \gamma * M_v \tag{7}$$

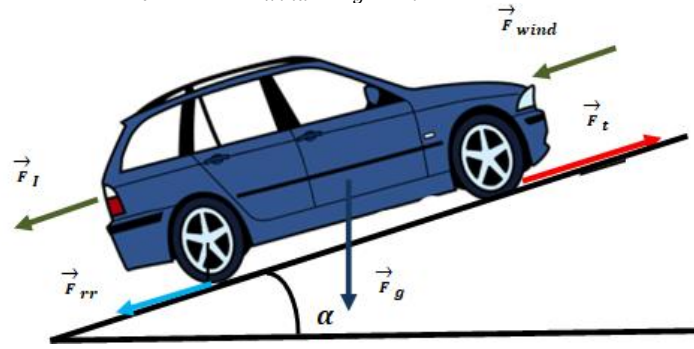Total forces resistances: $F_t = F_{rr} + F_{wind} + F_g + F_l$ (8)

Figure 2. Forces applied on the EV [19]

The longitudinal forces of the four drive wheels are calculated as (9) [10].

$$F_{ti} = \frac{\delta * M_v}{4} * \mu_i * cos(\alpha_p) \ \ i \in [1,4] \tag{9}$$

The resistive torque is calculated as (10) and (11) [10].

$$T_{ri} = F_{ti} * R_\omega - N_f * d_z \ \ i \in [1,3] \tag{10}$$

$$T_{ri} = F_{ti} * R_\omega - N_r * d_z \ \ i \in [2,4] \tag{11}$$

Where N_f and N_r are determined by (12) and (13) [10].

$$N_f = \frac{g * M_v}{2} \left(\frac{L_r}{L} - \frac{h_{cg}}{L_g} * \frac{dv_{cg}}{dt} * \alpha_p - \frac{h_{cg}}{L} * \alpha_p \right) \tag{12}$$

$$N_r = \frac{g * M_v}{2} \left(\frac{L_r}{L} + \frac{h_{cg}}{L_g} * \frac{dv_{cg}}{dt} * \alpha_p - \frac{h_{cg}}{L} * \alpha_p \right) \tag{13}$$

The linear model gives the front and rear forces [10].

$$F_{yf} = -C_f * \alpha_f \tag{14}$$

$$F_{yf} = -C_r * \alpha_r \tag{15}$$

The expressions of sideslip angles, longitudinal slip, and the relation between the sliding and tensile forces are given as (16) and (17) [10].

$$\alpha_f = -\delta + tan^{-1} \left(\frac{v_y + r * l_f}{v_x} \right) \tag{16}$$

$$\alpha_r = tan^{-1} \left(\frac{v_y - r * l_f}{v_x} \right) \tag{17}$$

Therefore, the longitudinal slip is given as (18).

$$\lambda_i = \frac{R_\omega * \omega_i - U_{ti}}{\max (R_\omega * \omega_i - U_{ti})} \ \ i \in [1,4] \tag{18}$$

Then, the relationship between λ and μ(traction coefficient) can be expressed as (19) [20]-[23].

$$\mu = C_1 * [\sin (C_2 * tan^{-1} \left(-C_4 * \left(C_3 * \lambda - tan^{-1}(C_3 * \lambda) \right) \right))] \tag{19}$$

2.3. The IM traction scheme

The torque function depends on the stators and rotor's currents as indicated in [8]:

$$\dot{X} = A.X + B.U$$

$$\dot{X} = \begin{pmatrix} \dot{I}_{s\alpha} \\ \dot{I}_{s\beta} \\ \dot{\emptyset}_{r\alpha} \\ \dot{\emptyset}_{r\beta} \end{pmatrix} ; B = \begin{pmatrix} \frac{1}{\sigma*L_s} & 0 \\ 0 & \frac{1}{\sigma*L_s} \\ 0 & 0 \\ 0 & 0 \end{pmatrix} ; U = \begin{pmatrix} V_{s\alpha} \\ V_{s\beta} \end{pmatrix} ; X = \begin{pmatrix} I_{s\alpha} \\ I_{s\beta} \\ \emptyset_{r\alpha} \\ \emptyset_{r\beta} \end{pmatrix}$$

$$A = \begin{pmatrix} -\frac{1}{\sigma*L_s}\left(R_s + \frac{Lm^2}{T_r*L_r}\right) & 0\frac{1}{\sigma*L_s}\left(\frac{Lm}{T_r*L_r}\right) & \frac{1}{\sigma*L_s}\left(\frac{Lm}{L_r}\right)\omega \\ 0 \quad -\frac{1}{\sigma*L_s}\left(R_s + \frac{Lm^2}{T_r*L_r}\right) & -\frac{1}{\sigma*L_s}\left(\frac{Lm}{T_r*L_r}\right)\omega & \frac{1}{\sigma*L_s}\left(\frac{Lm}{T_r*L_r}\right) \\ \frac{Lm}{T_r} & 0 - \frac{1}{T_r} & -\omega \\ 0 \quad \frac{Lm}{T_r}\omega & -\frac{1}{T_r} \end{pmatrix}$$

The electromagnetic torque Cem and the mechanical equation are given in [8]:

$$C_{em} = \frac{3}{2}p\frac{Lm}{L_r}(\dot{\emptyset}_{r\alpha}.\dot{I}_{s\beta} - \dot{\emptyset}_{r\beta}.\dot{I}_{s\alpha})$$

$$\frac{1}{p}J\frac{d\omega}{dt} = C_{em} - C_r - C_f$$

2.4. The inverter model

The inverter which has been use is used for the EV is the two-voltage type. It allows obtaining balanced alternating currents for various frequencies. The following matrix form gives details of the voltages generated and the logical switches' values as given in [8]:

$$\begin{pmatrix} V_{an} \\ V_{bn} \\ V_{cn} \end{pmatrix} = \frac{1}{3}U_{dc}\begin{pmatrix} 2 & -1 & -1 \\ -1 & 2 & -1 \\ -1 & -1 & 2 \end{pmatrix}\begin{pmatrix} S_a \\ S_b \\ S_c \end{pmatrix}$$

2.5. The electronic differential model

The electric vehicle, as seen in Figure 3, maintains the speeds of both drive wheels at the same value. In the case of a curvilinear path (left or right bend), the wheel steering angle is δ, which increases the speed of the wheel on the outside of the curve. In this way, the tires do not lose grip [8]. The parameters ω_R^* and ω_L^* represent the drive speeds of the actuators, respectively [12], [13]. For δ < 0, the EV turns to the left, δ > 0 turns to the right, δ = 0 goes straight ahead. The angular velocities of the drive wheels are:

$$\omega_R^* = (\frac{Vh}{R_\omega} - \frac{\Delta_\omega}{2}) \tag{20}$$

$$\omega_L^* = (\frac{Vh}{R_\omega} + \frac{\Delta_\omega}{2}) \tag{21}$$

Thus, the difference between the angular speed of the wheels is given by (22) [24], [25].

$$\Delta_\omega = \frac{d_\omega*\tan(\delta)}{(L_f + L_r)} * \frac{Vh}{R_\omega} \tag{22}$$

2.6. The variable master slave control model

This switchable control system offers the possibility to regulate the stator flow of the IM placed in parallel, thanks to a power supply to the wheels by a single converter. In some cases, IMs may be subject to

different charges. For this purpose, one of the machines can see its saturated magnetic circuit. In order to avoid this fate, it is imperative that the strategy being used be an effective means by which the voltage vectors delivered by the converter are distributed to each machine in a fair way, allowing them to develop adequate speeds and torques [10].

It is therefore a question here to regulating the flow of the stator of one machine at a time. One machine will be called the master, and thus makes the other a slave. The machine whose flow will be controlled will be called the master, and the other the slave. The torque of the master machine is the weakest. Thus, increasing the torque of a machine is followed by a decrease in its stator flux and vice versa, as follows in Figure 4.
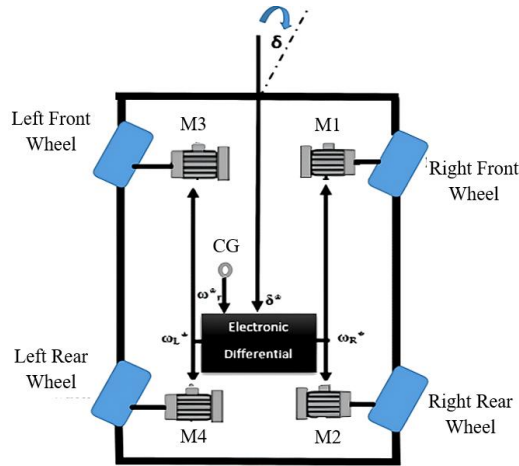
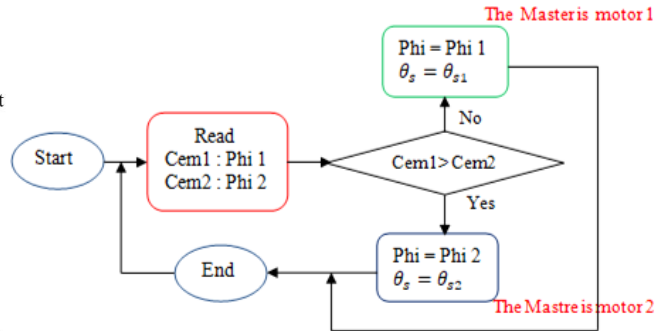Figure 3. Forces applied on the EV [10]   Figure 4. VMSC scheme

3.   HYBRID ARCHITECTURE AND CONTROL STRATEGY

This proposed strategy combines fuzzy logic and an adaptive neuro-fuzzy inference system (ANFIS). It should be noted here that it is developed for two motors located on either side (right or left) of the EV, and the entries of the hybrid controller are the output of the VMSC. Figure 5 shows its general architecture.

3.1. The adaptive neuro-fuzzy inference system (ANFIS) concept and learning algorithm

The generic ANFIS control structure has some components as a Takagi-Sugeno fuzzy inference system (FIS) with the exception of the neural network block. The network structure consists of five layers of units (and connections). Fuzzification, knowledge base, neural network, and defuzzification are the four main components of the proposed ANFIS controller. The proposed ANFIS controller has two inputs e and ed, and one output u. The corresponding ANFIS architecture is shown in Figure 6 [26].

Thus, the rule base contains i fuzzy rules of Takagi-Sugeno type:

$$\text{Rule 1 : If } e \text{ is } A_1 \text{ and } ed \text{ is } B_1, \text{then: } f_1 = p_1 * e + q_1 * ed + r_1, \tag{23}$$

$$\text{Rule 1 : If } e \text{ is } A_i \text{ and } ed \text{ is } B_i, \text{then: } f_i = p_i * e + q_i * ed + r_i, \tag{24}$$

Layer 1: In the same layer, the functions of the node remain the same function family, as shown:

$$O_{1;i} = \mu_{A_i}(e) \tag{25}$$

where e is the node i input and A_i is the linguistic label for this node. In other words, $O_{1;i}$ is the membership function (MFs) of A_i, and it specifies the membership degree of e to A_i. Trapezoidal, Triangular, or Gaussian are the most MFs used.

Layer 2: Each node in this layer is a circle node labeled II, which is used to obtain the activation degree of the premises. For instance:

$$w_i = \mu_{A_i}(e) * \mu_{B_i}(ed) \tag{26}$$

this layer's node function can be any T-norm operator that performs generalized AND.

Improved hybrid DTC technology for eCAR 4-wheels drive (Njock Batake Emmanuel Eric)

Layer 3: This layer has the rule to normalize the degree of activation of the rules. In it, each neuron is a circle neuron noted N. The ith neuron calculates the ratio between i^{th} rule weights and the sum of all rule weights.

$$\bar{w}_i = \frac{w_i}{w_1 + w_2 + \cdots + w_j} \qquad for\ i = 1,2 \dots, j \tag{27}$$

The operation above is the normalization of the rules of weights.

Layer 4: This layer is used to obtain the parameter set (p,q,r) of the rules. The function of this neuron is:

$$O_{1,4} = \bar{w}_i * f_i = \bar{w}_i (p_i * e + q_i * ed + r_i) \tag{28}$$

Layer 5: it is represented by a circle node labeled, which computes the total output as the sum of incoming signals. Thus:

$$O_{1,5} = u = \sum_i \bar{w}_i * f_i = \frac{\sum_i w_i * f_i}{\sum_i w_i} \tag{29}$$

we note that ANFIS is an FIS, whose MF parameters are adjusted using the back-propagation learning algorithm, or hybrid method algorithm (combination of BACK PROPAGATION AND LEAST MEAN SQUARED ERROR METHOD in training FIS Optima) option in MATLAB/Simulink when writing "anfisedit" in the command window block. After applying the hybrid method, the RMSE allows us to judge the quality of the effectiveness of the method used [10].
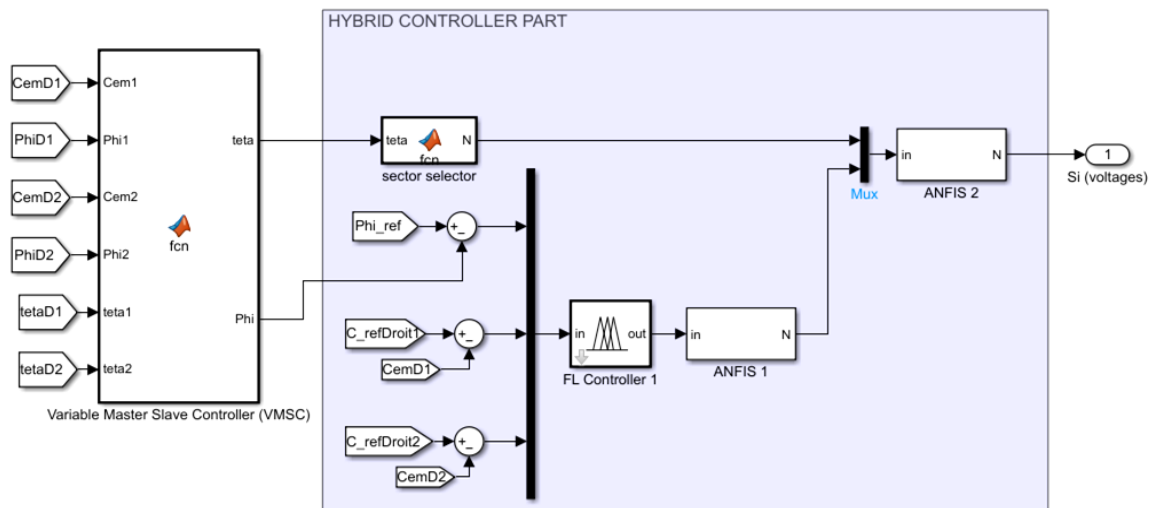

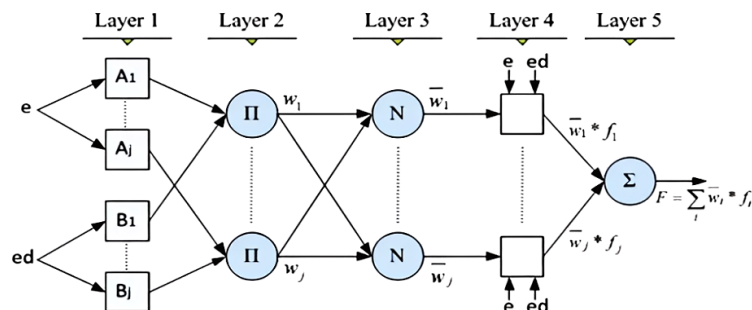Figure 5. Architecture of the hybrid controller part scheme

Figure 6. Structure of ANFIS controller [26]

3.2. Hybrid control method part

The control technique proposed in this article is the DTC associated with ANFIS and fuzzy logic. The block is shown in Figure 1 above. The hybrid regulator is made of 4 inputs, which are:

− ε_φ : Difference between the reference estimated stator flux and the stator flux.
− ε_{T1} : Difference between the reference torque and the electromagnetic torque of motor 1.
− ε_{T2} : Difference between the reference torque and the electromagnetic torque of motor 2.
− θ_s : Position of the stator flux. The HyC-DTC has its structure as shown in Figure 5 above.

It is made of an electromagnetic torque regulation based on a Mandani-type fuzzy regulator FL controller 1. Thus, it includes two inputs:

− $\varepsilon_{T1} = CemRef1 - Cem1$ for motor 1
− $\varepsilon_{T2} = CemRef2 - Cem2$ for motor 2
− $\varepsilon_\varphi = \varphi Ref - \varphi$
−   The universe of discourses set is:

> For ε_φ we have: $H = \{$N (negative), z (Zero), P (positive).$\}$
> For $\varepsilon_{T1}, \varepsilon_{T2}$ we have: $E = \{$NG, NP, Z, PP, PG.$\}$

Where elements of E are membership functions of algorithm parameters of HyC-DTC given for the fuzzification as follows:

[Input1]
Name = 'E_{phi}'
Range = [-1.5 1.5]
NumMFs = 3
MF1 = 'N':'trapmf',[-2 -1.5 -0.01 0]
MF2 = 'Z':'trimf',[-0.01 0 0.01]
MF3 = 'P':'trapmf',[0 0.01 1.5 2]

[Input 1 OR 2] I = {1,2}
Name = 'E_{Cemi}'
Range = [-10000 10000]
NumMFs = 5
MF1 = 'NG':'trapmf',[-15000 -10000 -2 -1]
MF2 = 'NP':'trimf',[-2 -1 0]
MF3 = 'Z':'trimf',[-1 0 1]
MF4 = 'PP':'trimf',[0 1 2]
MF5 = 'PG':'trapmf',[1 2 10000 15000]

The hybrid method proposed here is inspired by the FDTC of [8]. In the FDTC, we distinguish one controller of fuzzy Mamdani type, which has 2 inputs ε_{T1} and ε_{T2} for 2 motors on the same side and returns an output V. A second fuzzy Mamdani-type controller that takes input ε_φ and returns an output U. A sector generator that takes at its input the angle θ_s and returns an output N. It is quickly noticed from the table of bases adopted in the FDTC that all the values taken by V are found in E.

For the HyC-DTC $\varepsilon_{T1}, \varepsilon_{T2}, \varepsilon_\varphi$ are the inputs of a fuzzy Mamdani controller type FL1. FL1 returns an output V. A sector selector gives the outputs membership functions (MFs) θ_j by taking the input values of the stator flux position θ_s. To better understand the previous comments and establish the laws of FL1, it should be noted that for the HyC-DTC, the combination ε_{T1} and ε_{T2} are those given in Table 1.

In addition, there are also some combinations between ε_{T1} and ε_{T2} in Table 1, which are given the same values of V or which are repeated. For example, if both combinations ($\varepsilon_{T1} = NG$ and $\varepsilon_{T2} = NG$ then $V = NG$) ; if ($\varepsilon_{T1} = NG$ and $\varepsilon_{T2} = NP$ then $V = NG$) will get the same number as 5, for example. Laws can thus be made to FL1, which are triplets ($\varepsilon_\varphi, \varepsilon_{T1}, \varepsilon_{T2}) \in H * E * E$. Any triplet of which combination of ε_{T1} and ε_{T2} have the same numbers will be grouped in membership Classes O_i. We thus can make a group of couples ($\varepsilon_{T1}, \varepsilon_{T2}$) according to the numbers $n = \{1,2,3,4,5\}$ and triplets ($\varepsilon_\varphi, \varepsilon_{T1}, \varepsilon_{T2}$) according to Classes $O_i (i\epsilon\{1,2; ...,15\})$ following Figure 7 and Table 2.

Thus, it can be remarked that the triplets (N, NG, PG), (N, Z, Z), (N, PG, NG) have the same class O_3, because the three couples (NG, PG), (Z, Z), and (PG, NG) have the same number 3 in Figure 7. It should also be mentioned that the number of the class and the number given to a couple that is included in this triplet are not necessarily the same. For example, (NG, NG) and (NG, NP) have the same number affected, 5, but (N, NG, NG) and (N, NG, NP) have the same membership Class O_3.

Table 1. Combination table for torque error MFs

$\varepsilon_T = \varepsilon_{Tj}/\varepsilon_{Tj+1}$	NG	NP	Z	PP	PG
NG	<NG>	<NG>	<NP>	<NP>	<Z>
NP	<NG>	<NP>	<NP>	<Z>	<PP>
Z	<NP>	<NP>	<Z>	<PP>	<PP>
PP	<NP>	<Z>	<PP>	<PP>	<PG>
PG	<Z>	<PP>	<PP>	<PG>	<PG>

Table 2. MFs O_i generated by Fuzzy1

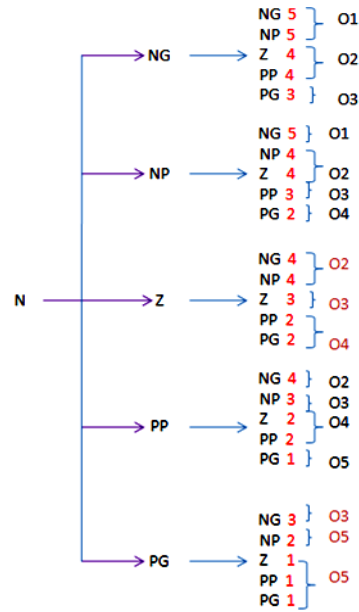| $\varepsilon_T/\varepsilon_\varphi$	<NG>	<NP>	<Z>	<PP>	<PG>
N	O_1	O_2	O_3	O_4	O_5
Z	O_6	O_7	O_8	O_9	O_{10}
P	O_{11}	O_{12}	O_{13}	O_{14}	O_{15}

Figure 7. Illustration of triplets $(N, \varepsilon_{T1}, \varepsilon_{T2})$, the numbering of a couple $(\varepsilon_{T1}, \varepsilon_{T2})$ and the O_i classes

Thus, the change to another triplet tree of type $(z, \varepsilon_{T1}, \varepsilon_{T2})$ or $(P, \varepsilon_{T1}, \varepsilon_{T2})$ like $\varepsilon_\varphi \in H$ occurs. One increments the layer of a larger number of the previous layer. The same reasoning starts again. Figures 8 and 9 are as follows:
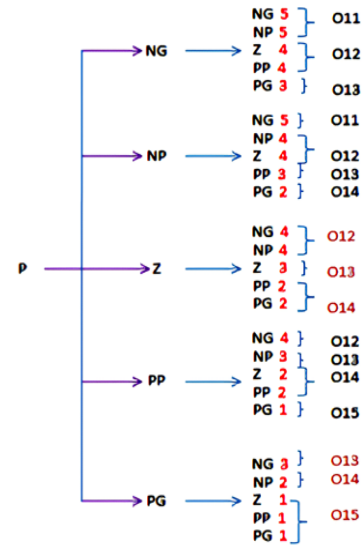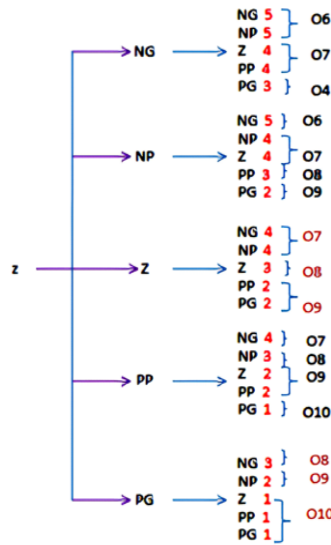

Figure 8. Triplets $(z, \varepsilon_{T1}, \varepsilon_{T2})$ and their classes   Figure 9. Triplets $(P, \varepsilon_{T1}, \varepsilon_{T2})$ and their classes

The corresponding data for the outputs $O_i (i \epsilon \{1,2; ..., 15\})$ are made up as follows:

[Output1]
Name='O'
Range=[0 16]
NumMFs=15
MF1='O1':'trimf',[0.5 1 1.5]   MF2='O2':'trimf',[1.5 2.001 2.5]
MF3='O3':'trimf',[2.5 3 3.5]   MF4='O4':'trimf',[3.5 4 4.5]

We remarked that every Class $O_i (i \epsilon \{1,2; ... ,15\})$ is linked to an interval [i-0.5 i i+0.5]. Thus, for the class O_{15} we have: MF15='O15':'trimf', [14.5 15 15.5].

Further, the development of this work has encountered a problem that had to be solved. Indeed, the controller FL1 or fuzzy controller 1 does not provide in its laws values of couples that exist fine and well in the instructions but whose occurrence can not materialize. To overcome this random discontinuity, it was necessary to use a second Blur controller of type Sugeno, this time if which will take the outputs of FL1 as inputs and generate a new membership function taking into account the intervals in which fuzzification is not carried out. It should be noted that, this Sugeno controller will then be coupled to a block "To Workspace" to generate the corresponding ANFIS-type controller compatible with Sugeno type and validated further thanks to a consistent RMSE and the Save 2-D signals as: 3-D array (concatenate along third dimension). This is illustrated in Figure 10.
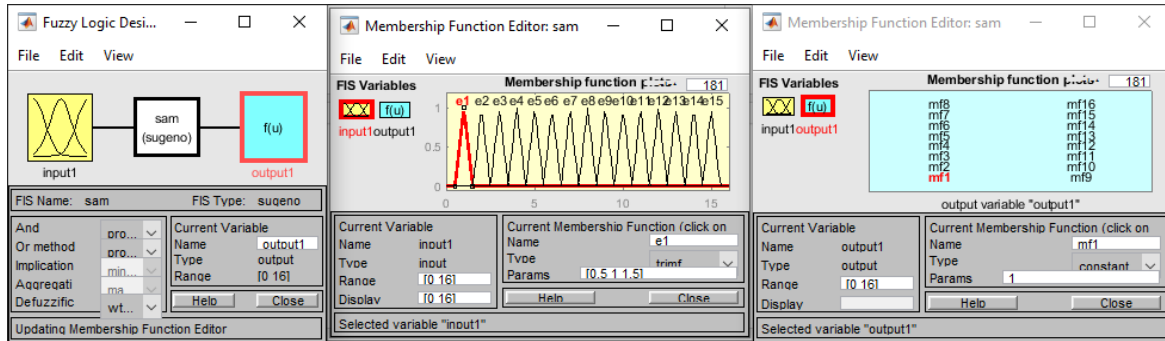
Figure 10. A given aspect of the Sugeno fuzzy controller

Then we proceeded to a read algorithm using the ANFIS model. The inputs of the ANFIS controller are the $e_i (i \epsilon \{0,1,2; ... ,15,16\})$ as shown in Figure 10 on the left, and the outputs of the controller are the function $mf_j (j \epsilon \{0,1,2; ... ,15,16\})$ as shown in Figure 10 on the right. This is an ANFIS 1 controller that overcomes some of the FL1's defects.

Figure 11 gives the inputs and outputs MFs type and range of the ANFIS 2 controller. In addition, as inspired by [8], the generation of sectors θ_k or θ_j is done according to 12 MFs, as seen on Figure 11(a). These MFs are the 12 classes of values taken by the outputs from the sector selection block shown in Figure 11(b). A second algorithm that uses the hybrid option and RMSE in MATLAB/Simulink 2021a allows to design of the second ANFIS controller named ANFIS 2. This learning algorithm has 2 inputs, θ_j of the bloc sector selector expressed on Figure 11(b) (MFs of range [0 12]) and e_i (which is the output of the bloc ANFIS 1) expressed on Figure 11(c) (MFs of range [0 15]). The output "e" of ANFIS 2, as seen on Figure 11(d) (MFs of range [0 7]), are vectors V_i which come from the combinations of a quadruplet (ε_T1,ε_T2, 〖 ε〗 _φ,θ_k). Each vector value V_i corresponds to a triplet (U_a,U_b,U_c) which is the output of the 2-level inverter. It should be remarked that the use of the learning algorithm of the hybrid and RMSE of ANFIS will not be possible without the use of the block to workspace, and the save 2-D signals as: 3-D array (concatenated along the third dimension). All these purposes are shown in Figure 11.

Table 3 summarizes the state of the output vector V_i obtained from values delivered by ANFIS1 and the sector selection block used to power the inverter. This is used to model ANFIS 2 using the hybrid learning method, thanks to the block used after entering ''anfisedit'' in MATLAB for a program $V_i = i$.

Therefore, for it can be established a correspondence between V_i values and triplet (U_a, U_b, U_c)_ of the inverter. Then we have quadruplet : (V0,0;0;0);(V1,2*U/3;-U/3;-U/3);(V2,U/3;U/3;-2*U/3);(V3,-U/3;2*U/3;-U/3);(V4,-2*U/3;U/3;U/3);(V5,-U/3; U/3;2*U/3) ;(V6,U/3;-2*U/3;Vc=U/3);(V7,0;0;0). U is a continuous voltage at the entrance to the inverter. Generated Rules of ANFIS 2 controller made by the learning algorithm of the Sugeno file from ANFIS:

1. If (input1 is in1mf1) and (input2 is in2mf1) then (output is out1mf1) (1)
2. If (input1 is in1mf1) and (input2 is in2mf2) then (output is out1mf2) (1)
3. If (input1 is in1mf1) and (input2 is in2mf3) then (output is out1mf3) (1)
...
178. If (input1 is in1mf12) and (input2 is in2mf13) then (output is out1mf178) (1)
179. If (input1 is in1mf12) and (input2 is in2mf14) then (output is out1mf179) (1)
180. If (input1 is in1mf12) and (input2 is in2mf15) then (output is out1mf180) (1)
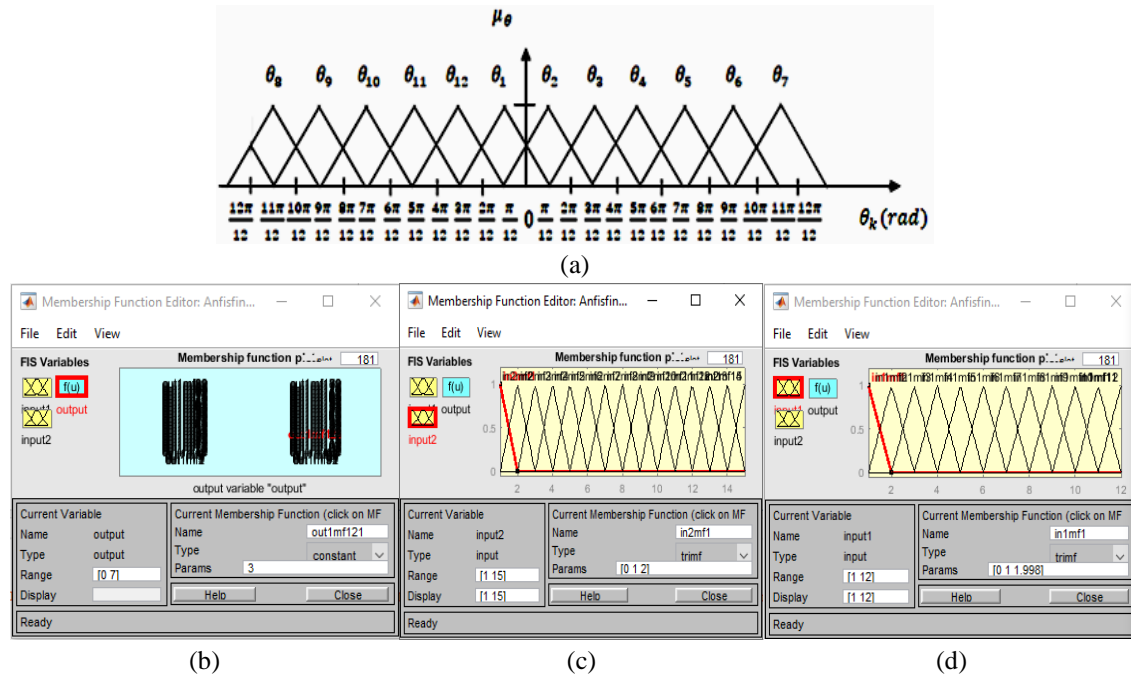It can be remarked that, back propagation, least square algorithm are described in MATLAB/Simulink.

(a)

(b)   (c)   (d)

Figure 11. Inputs, outputs variables of ANFIS 2: (a) MFS angles θ_k, (b) vector V_i , (c) MFS e_i, and (d) MFS θ_j

Table 3. Synthesis of the output vector used to model the controller ANFIS2 [27], [28]

	θ_1	θ_2	θ_3	θ_4	θ_5	θ_6	θ_7	θ_8	θ_9	θ_{10}	θ_{11}	θ_{12}
o_1	V1	V2	V2	V3	V3	V4	V4	V5	V5	V6	V6	V1
o_2	V2	V2	V3	V3	V4	V4	V5	V5	V6	V6	V1	V1
o_3	V0	V7	V7	V0	V0	V7	V7	V0	V0	V7	V7	V0
o_4	V6	V6	V1	V1	V2	V2	V3	V3	V4	V4	V5	V5
o_5	V6	V6	V1	V1	V2	V2	V3	V3	V4	V4	V5	V5
o_6	V2	V2	V3	V3	V4	V4	V5	V5	V6	V6	V1	V1
o_7	V2	V3	V3	V4	V4	V5	V5	V6	V6	V1	V1	V2
o_8	V7	V0	V0	V7	V7	V0	V0	V7	V7	V0	V0	V7
o_9	V7	V0	V0	V7	V7	V0	V0	V7	V7	V0	V0	V7
o_{10}	V5	V6	V6	V1	V1	V2	V2	V3	V3	V4	V4	V5
o_{11}	V2	V3	V3	V4	V4	V5	V5	V6	V6	V1	V1	V2
o_{12}	V3	V3	V4	V4	V5	V5	V6	V6	V1	V1	V2	V2
o_{13}	V0	V7	V7	V0	V0	V7	V7	V0	V0	V7	V7	V0
o_{14}	V4	V5	V5	V6	V6	V1	V1	V2	V2	V3	V3	V4
o_{15}	V5	V5	V6	V6	V1	V1	V2	V2	V3	V3	V4	V4

4. RESULTS AND DISCUSSION

The simulation parameters used in this paper were chosen after an investigation of the thesis work of [25] with prototyping, but also of [6] and [28].

4.1. Simulation of the hybrid system and the FDTC during 2 s

The FDTC figures and results are taken from [17]. For each method, a load of 30 k.N is applied to two IMs on the same side at intervals of 0.4 to 0.8s for the first, then 1.2s to 1.6s for the second. Figures 12(a) and 12(b) give an overview of the speeds of the front right and rear motors used respectively in the FDTC and hybrid approach, for a reference of 100 rad/s with a load of 30 k.N. Figure 12(a) reveals that the FDTC has a faster response than the hybrid. Figure 12(b) shows that the hybrid approach is more accurate than FDTC, and a very small overshoot. Figure 12(c) gives a zoom of the graph obtained by the hybrid approach.

However, on closer inspection, it can be seen that the proposed control is much more accurate than the FDTC and has a very low torque ripple rate (5 times lower) of the induction machines used compared to that of the FDTC (Figures 13(a) and 13(b)). The rising time of HyC makes the transient period longer.
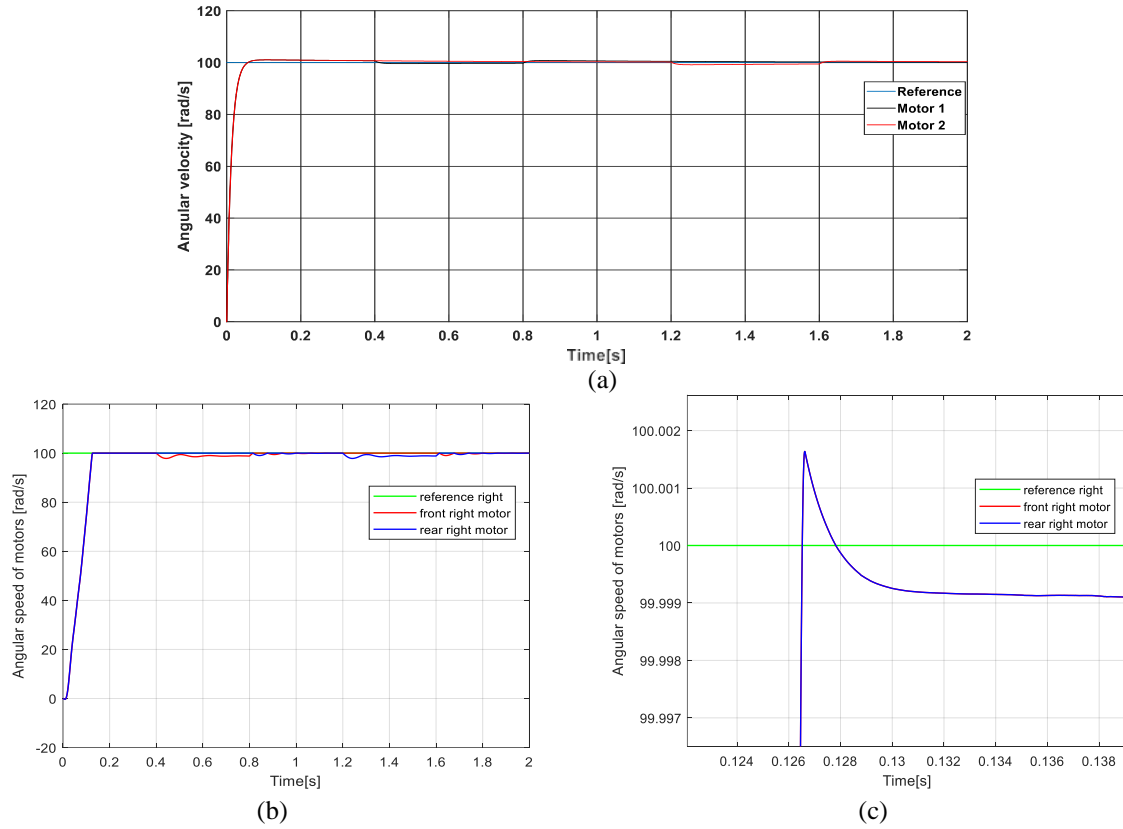
Figure 12. Angular speed: (a) FDTC, (b) hybrid, and (c) zoom of hybrid
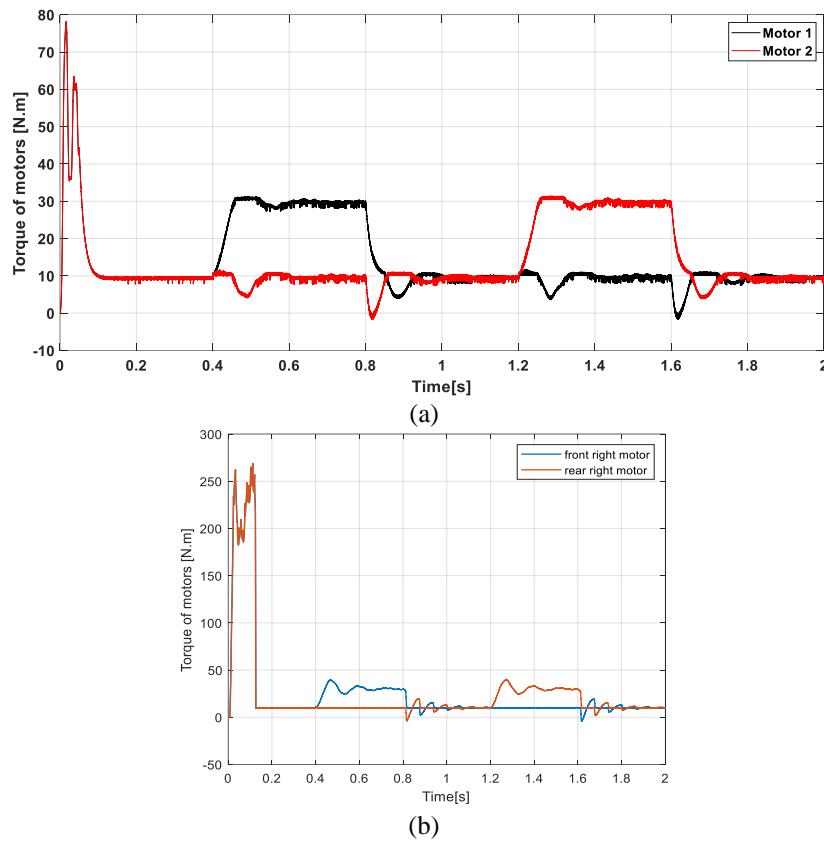

Figure 13. Torque: (a) FDTC and (b) hybrid

Figures 14(a) and 14(b) illustrate the circulation of the flux along the alpha-beta axes by two circles of radius 1(value of the reference flux 1 Wb). the profile of both circles shows that the hybrid method (Figure 14(b)) is a more refined flux signal than the FDTC method (Figure 14(b)). Figure 14(c) represents the graph of the change in stator flux in both motors of the same side over time. The magnetic stability of the flux, which is remarkable here, is ensured by the VMSC module.

(a)   (b)

(c)
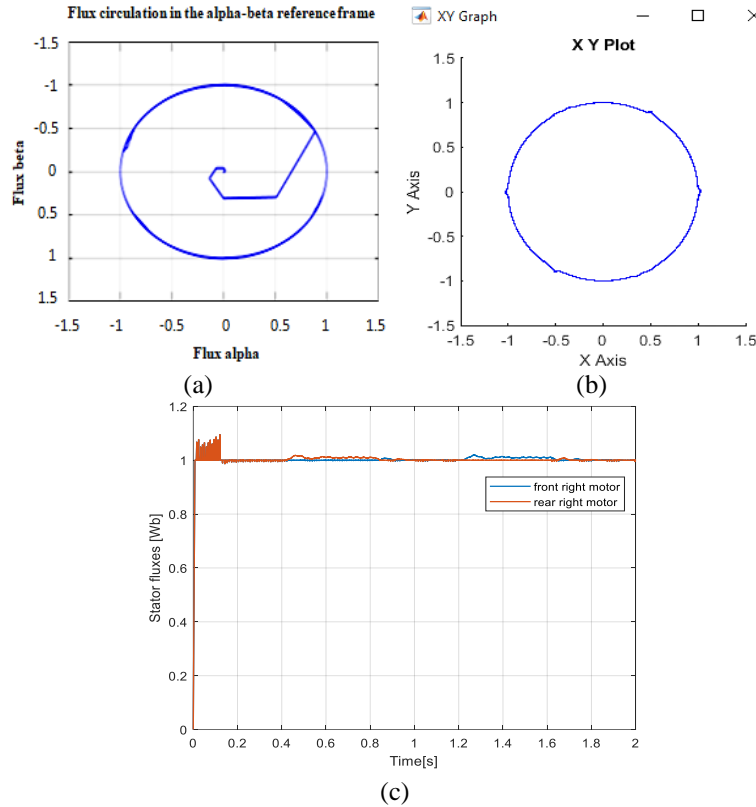
Figure 14. The circulation of stator flux: (a) FDTC, (b) hybrid, and (c) stator flux variation over time

Figure 15 shows the three-phase current curves of the induction machines during this test. Between 0 and 2 seconds, a torque of traction is given to the vehicle. During this period, it can be observed that, Figure 15(b) has a larger area of disturbance than Figure 15(a). It is due to the transient regime, which is longer for the hybrid approach than the FDTC, respectively.

4.2. Simulation of the hybrid system and the FDTC for the EV during 20 s

The simulation parameters of the systems, the VMSC structure technique and its structure, the FDTC approach, are fully details in [17]. Motors provide high tractive forces to move the vehicle from the start to overcome the forces of overall resistance of the EV movement, to ensure the stability of the vehicle. It is observed in Figure 16(a) that the oscillations are greater with the FDTC compared to the hybrid method. The torque ripples have been greatly reduced in the hybrid system, as shown in Figure 16(b), from approximately [-0.5, 0.5] in FDTC to [-0.1, 0.1]. Furthermore, Figure 16(c) presents a zoomed view of Figure 16(b) between 14.98 and 15.08 s, which makes it possible to assess more clearly the reduction in torque ripples of the hybrid method. Here, a good tracking of torque references can be observed, which testifies to the robustness of the control. Thus, with the hybrid approach, it is possible to reduce the vibrations of the motor shaft and noise, which have the effect of reducing the life of the various engines while ensuring a certain comfort in the passenger compartment. This can justify the choice of the hybrid method.

The stator fluxes of each of the machines follow their reference despite multiple variations in torque. Figure 13 shows that the flux ripples are more important in the FDTC (Figure 17(a)) than hybrid method (Figure 17(b)). The robustness of this control strategy is once observed, in spite of the external disturbance.
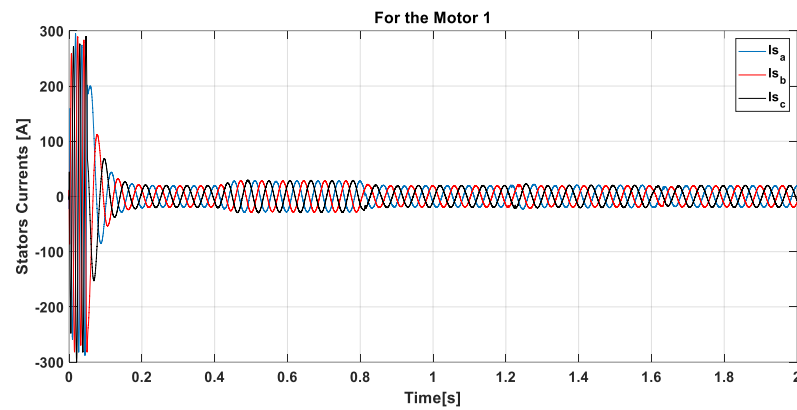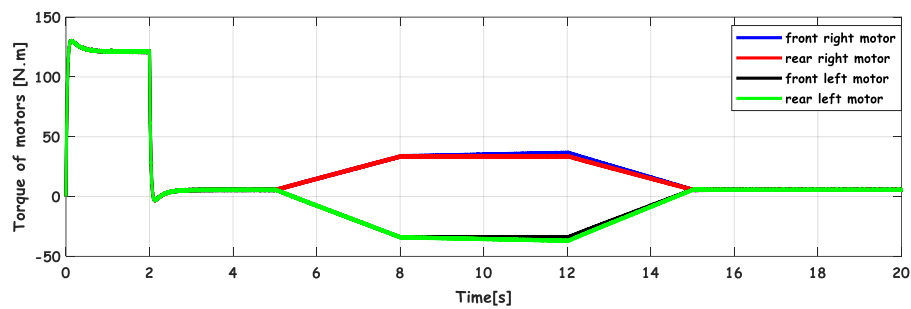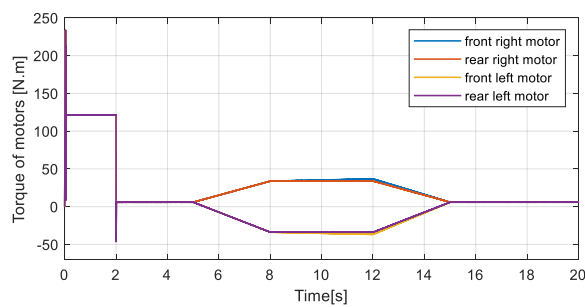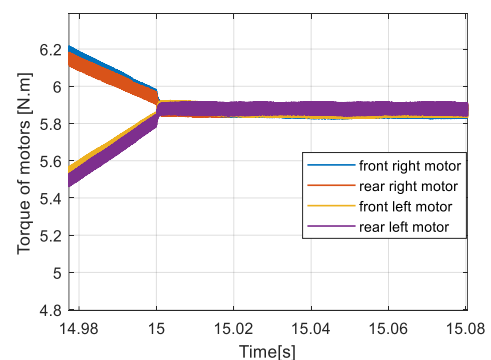
(a)
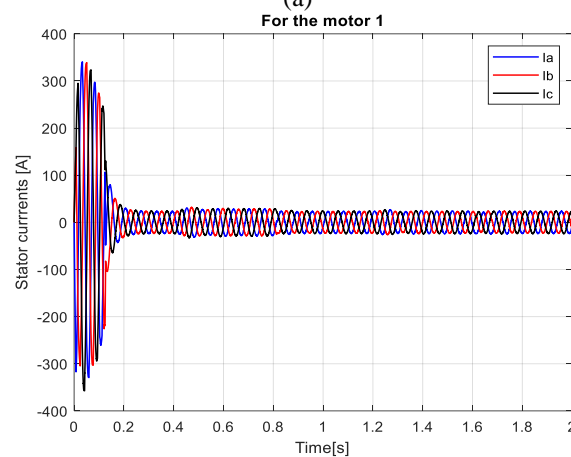
(b)

Figure 15. Stator currents: (a) FDTC and (b) hybrid

(a)

(b)

(c)

Figure 16. Torque of motors: (a) FDTC, (b) hybrid method, and (c) zoom of hybrid method
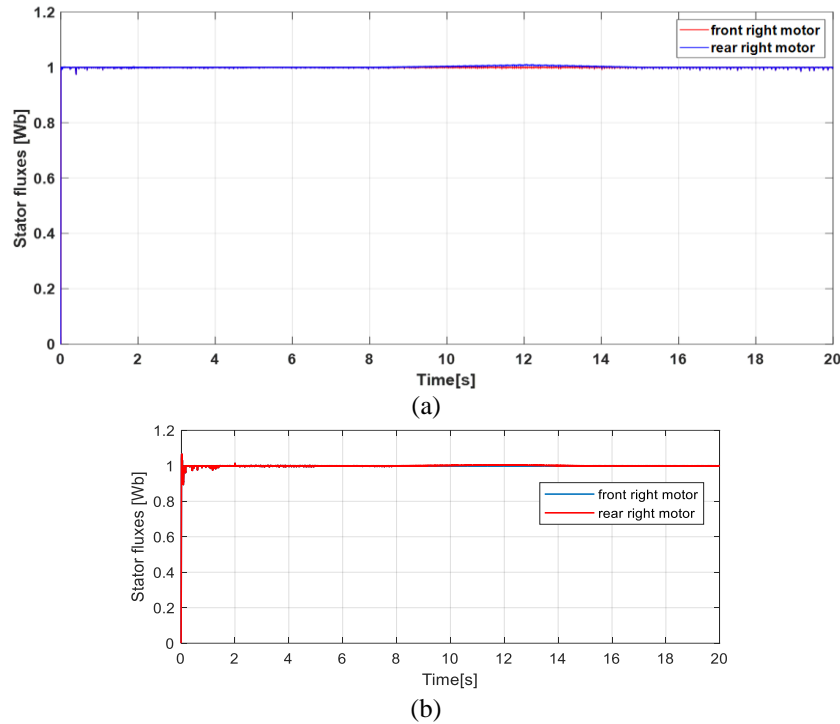
(a)

(b)

Figure 17. Stator fluxes: (a) FDTC and (b) hybrid

Hybrid Figures 18(a) and 18(b) show the evolution of the stator currents absorbed by each motor for each control strategy used. Between 0 and 2 s, this is the starting phase, which is characterized by high current amplitudes reaching 80 A. The current amplitude becomes stable at 30 A, when the VE gets to it reference speed. During the rotation, the evolution of the current is linked to that of the electromagnetic torque developed by the corresponding motor, until it reaches a value of 50 A.

(a)

(b)
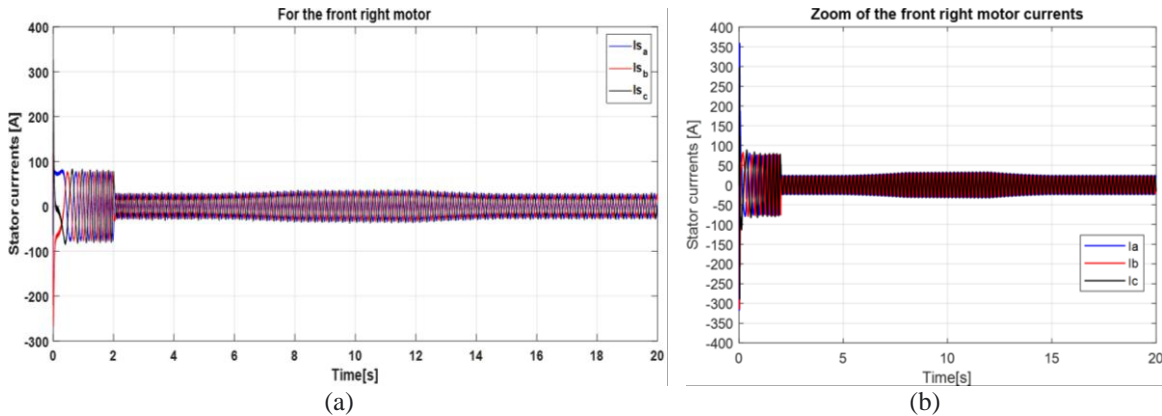
Figure 18. Stator currents: (a) FDTC and (b) hybrid

We see that after this phase, when the vehicle has reached its reference speed, the current amplitude stabilizes at 30 A. During the turn, the currents follow the evolution of the electromagnetic torque developed by the corresponding motor until reaching a value of 50 A. Figures 19(a) and 19(b) illustrate the zoom in on the currents allows you to appreciate their good waveform around 2.2 and 3 seconds, respectively, for the FDTC and hybrid approach. Both methods present a spectrum almost identical, but the hybrid method of Figure 19(b) presents the advantage of feeding motors under 180 V when the voltage required for the FDTC is 380 V.

Figure 20(a) shows the graphical evolution of angular speed and references. Figure 20(b) is a zoom of Figure 20(a). Between 8 and 12 seconds, there is a slight decrease in the speed of the rear left and front right wheels. This can be explained by the increase in resistive torque of 10 N.m during the journey of the EV.
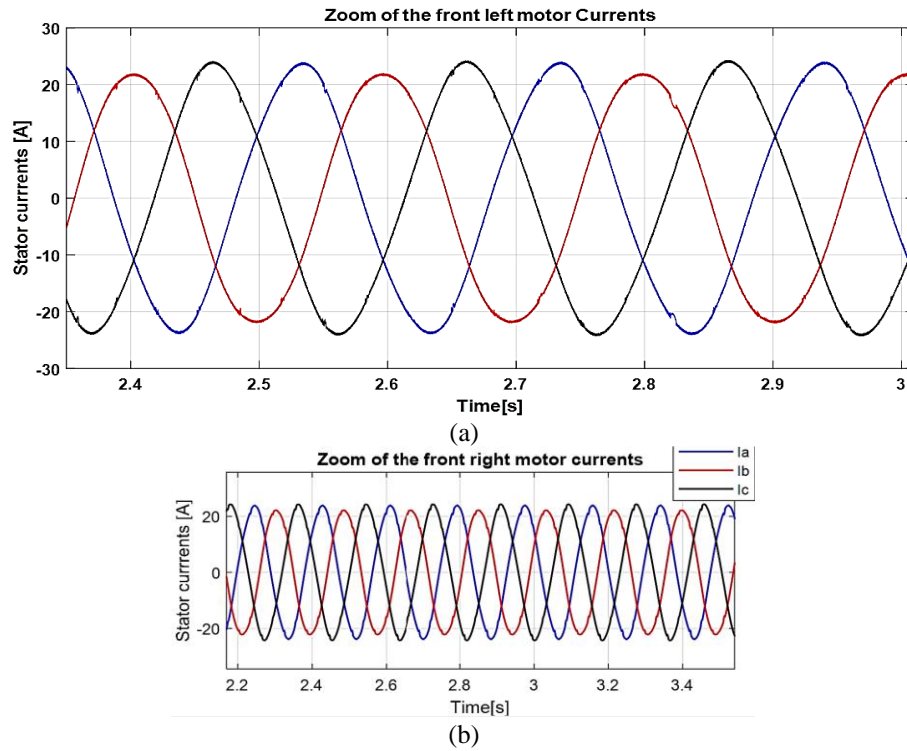
(a)

(b)

Figure 19. Zoom of stator currents: (a) FDTC and (b) hybrid
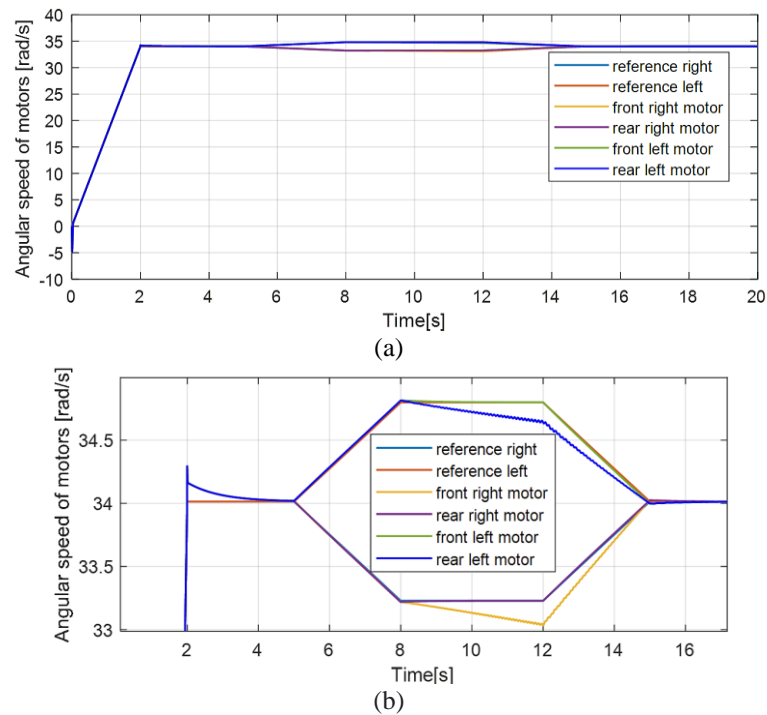

(a)

(b)

Figure 20. Angular speeds evolution of EV motors: (a) hybrid method and (b) zoom of angular speed

Figure 21 shows the root mean square error (RMSE) in the hybrid system of ANFIS 2 controllers and it ANN internal structure. With only 2 epochs, the hybrid method gives the RMSE of ANFIS2, is ANFIS2 is 1.24995^e-7. It can be justified that the controller operates quickly with better accuracy. Figure 22 shows the RMSE in the hybrid system of the ANFIS 1 controller and its ANN internal structure. With only 2

epochs, the hybrid method gives the RMSE of ANFIS 1 is 3.97653^e-08. It can justify that the controllers operate quickly with a great accuracy.
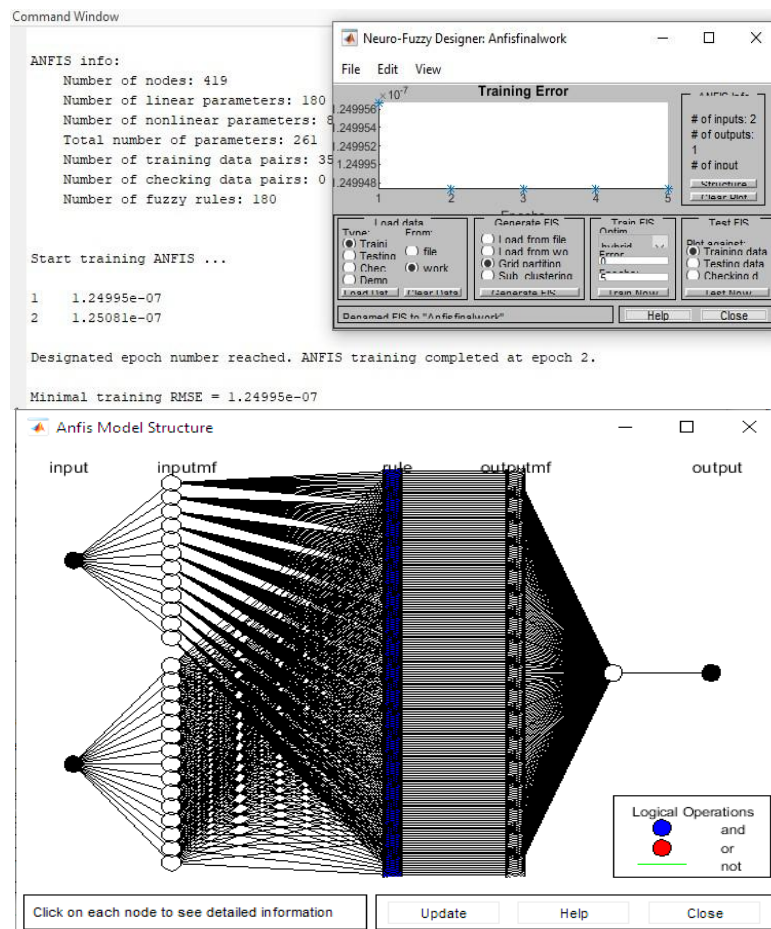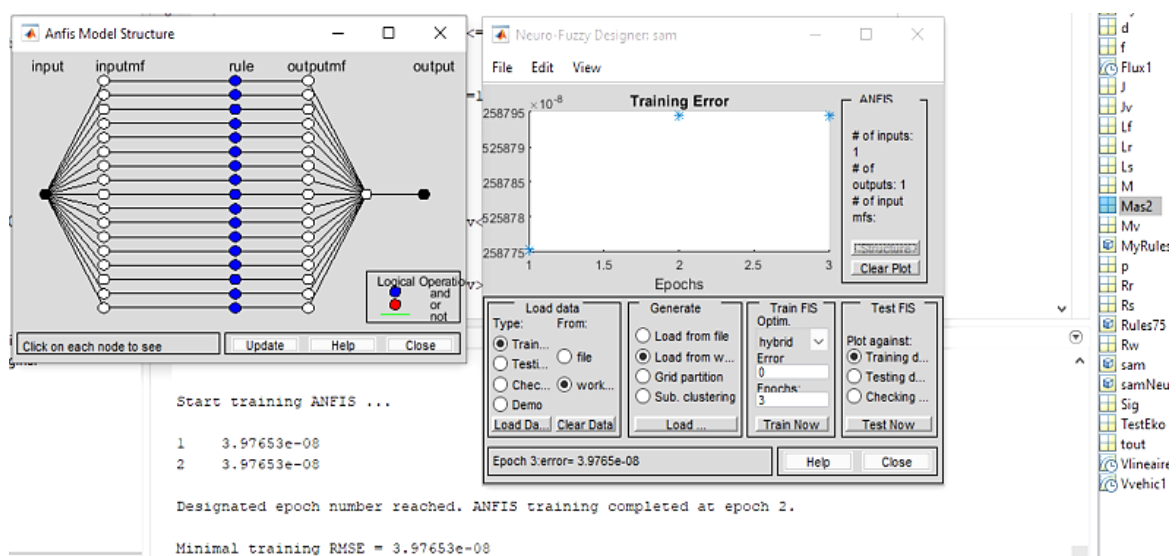

Figure 21. RMSE and ANN structure of ANFIS2

Figure 22. RMSE and ANN structure of ANFIS 1

4.3. Comparative studies of the two approaches

The previous simulations were based on two approaches, FDTC and hybrid for an EV. They have both shown their effectiveness in terms of the dynamic stability of the system highlighted in Figure 1 under various constraints on the same road. The justification and observation of the effects of disturbances on the EV were made possible by subjecting the system to two control approaches under identical conditions. The dynamic parameters resulting from this experiment are summarized in Table 4. Here FDTC has 4.5% reduction in rising time compared to the hybrid approach. Nevertheless, the hybrid method has a better signal quality profile, as it reduces torque oscillations by 40% from a range of [-0.5; 0.5] to [-0.1; 0.1] in Figure 12. This not only improves passenger comfort by reducing mechanical noise, but also extends the life of the equipment. In addition, the two approaches have the same static error margins, but it can be seen that the overshoot in the FDTC case is greater than that of the hybrid method, i.e. 19.6%, which could lead to the conclusion that the Hybrid method performs better than the FDTC in the current case.

Table 4. Performance of hybrid control and FDTC speed responses

Type of control	Rising time	Overshoot	Steady state error
Hybrid approach	0.075	0.496	0.00106
FDTC	0.03	0.692	0.001

5. CONCLUSION

In the present article, two methods of controlling multimachine systems are presented, and among the both, one is proposed. The EV architecture chosen is that of four wheels each with an IM. using two static converters to supply power to the motors. For the first approach, DTC is associated to FL and VMSC to master magnetic quantities and control the speed. The second method combine FL and Neuro-fuzzy (Hybrid ANFIS) and VMSC system with DTC. During the turning, the use of an electronic differential (ED) makes possible the management of magnetic quantities and speed, climbing, and descending phases. The HyC technics have proved his efficiency with respect to the FDTC by its dynamic's parameters obtained like 0.496 vs 0.692 of overshoot, and a same steady state error value 0.001 as the FDTC. The results show that HyC is more precise and refined than FDTC because it reduces significantly the Torque ripples as illustrated in FDTC. Unfortunately, the HyC has a problem simulation. Results show then that, HyC approach is a good approach for training multi-machine systems of EV, but the problem of the great rising time must be solve because it make long the transient response of the system with more ripple in the general view of the parameters of the EV.

AUTHOR CONTRIBUTIONS STATEMENT

This journal uses the Contributor Roles Taxonomy (CRediT) to recognize individual author contributions, reduce authorship disputes, and facilitate collaboration.

Name of Author	C	M	So	Va	Fo	I	R	D	O	E	Vi	Su	P	Fu
Njock Batake Emmanuel Eric	✓	✓	✓	✓	✓	✓	✓	✓	✓	✓	✓		✓	✓
Nyobe Yome Jean Maurice	✓	✓	✓	✓	✓	✓	✓	✓	✓	✓	✓	✓	✓	
Ngoma Jean Pierre	✓	✓		✓	✓		✓	✓	✓	✓	✓	✓		✓
Ndoumbé Matéké Max	✓	✓	✓	✓	✓	✓	✓	✓	✓	✓	✓	✓	✓	

C : **C**onceptualization	I : **I**nvestigation	Vi : **Vi**sualization
M : **M**ethodology	R : **R**esources	Su : **Su**pervision
So : **So**ftware	D : **D**ata Curation	P : **P**roject administration
Va : **Va**lidation	O : Writing -**O**riginal Draft	Fu : **Fu**nding acquisition
Fo : **Fo**rmal analysis	E : Writing - Review &**E**diting	

DATA AVAILABILITY

All the data that support the findings of this study are included within the article and any supplementary files.

REFERENCES

[1] M. I. Abdelwanis, "Optimizing the performance of six-phase induction motor-powered electric vehicles with fuzzy-PID and DTC," *Neural Computing and Applications*, vol. 37, no. 16, pp. 9721–9734, Jun. 2025, doi: 10.1007/s00521-024-10455-0.

[2] H. Tiwari, A. Ghosh, C. Sain, F. Ahmad, and L. Al-Fagih, "Modified direct torque control algorithm for regeneration capability of im driven electric vehicle by using hybrid energy storage system," *Renewable Energy Focus*, vol. 48, p. 100534, Mar. 2024, doi: 10.1016/j.ref.2023.100534.

[3] D. Mohanraj, J. Gopalakrishnan, B. Chokkalingam, and L. Mihet-Popa, "Critical aspects of electric motor drive controllers and mitigation of torque ripple—review," *IEEE Access*, vol. 10, pp. 73635–73674, 2022, doi: 10.1109/ACCESS.2022.3187515.

[4] G. Ge, L. Shi, K. Yang, and D. Tan, "Research status of electronic differential control of electric vehicle driven by in-wheel motor," *International Journal of Vehicle Safety*, vol. 11, no. 4, p. 289, 2020, doi: 10.1504/IJVS.2020.10033767.

[5] T. E. McWhirter, T. J. Wagner, J. E. Stubbs, D. M. Rizzo, and J. B. Williams, "Tracked vehicle physics-based energy modelling and series hybrid system optimisation for the Bradley fighting vehicle," *International Journal of Electric and Hybrid Vehicles*, vol. 12, no. 1, p. 1, 2020, doi: 10.1504/IJEHV.2020.104271.

[6] K. Houacine, R. Mellah, S. Guermah, and M. Charif, "Neural fuzzy control of driving wheels for electric vehicle," in *3rd International Conference on Systems and Control*, IEEE, Oct. 2013, pp. 25–30. doi: 10.1109/ICoSC.2013.6750830.

[7] K. Houacine, R. Mellah, and S. Guermah, "Compensatory neural fuzzy control for two wheels electric vehicle drive," *International Journal of Electric and Hybrid Vehicles*, vol. 7, no. 2, p. 189, 2015, doi: 10.1504/IJEHV.2015.071060.

[8] N. Matéké Max, N. Yome Jean Maurice, E. Samuel, B. Laurent, and A. Biboum, "Electric vehicle wheel drive analysis using direct torque fuzzy control method," *Conference: Solid State Technology: Electric Vehicle,* 2020, vol. 63, no. 5.

[9] M. Sekour, K. Hartani, and A. Merah, "Electric vehicle longitudinal stability control based on a new multimachine nonlinear model predictive direct torque control," *Journal of Advanced Transportation*, vol. 2017, pp. 1–19, 2017, doi: 10.1155/2017/4125384.

[10] N. M. Max *et al.*, "Artificial intelligence-enhanced DTC command methods used for a four-wheel-drive system," *International Journal of Power Electronics and Drive Systems (IJPEDS)*, vol. 14, no. 4, pp. 1983–1994, 2023, doi: 10.11591/ijpeds.v14.i4.pp1983-1994.

[11] Y. Sahri *et al.*, "Effectiveness analysis of twelve sectors of DTC based on a newly modified switching table implemented on a wind turbine dfig system under variable wind velocity," *Ain Shams Engineering Journal*, vol. 14, no. 11, 2023, doi: 10.1016/j.asej.2023.102221.

[12] F. V. A. Raj and V. K. Kannan, "Particle swarm optimized deep convolutional neural Sugeno-Takagi fuzzy PID controller in permanent magnet synchronous motor," *International Journal of Fuzzy Systems*, vol. 24, no. 1, pp. 180–201, Feb. 2022, doi: 10.1007/s40815-021-01126-6.

[13] R. Kumar, A. Baz, H. Alhakami, W. Alhakami, A. Agrawal, and R. A. Khan, "A hybrid fuzzy rule-based multi-criteria framework for sustainable-security assessment of web application," *Ain Shams Engineering Journal*, vol. 12, no. 2, pp. 2227–2240, Jun. 2021, doi: 10.1016/j.asej.2021.01.003.

[14] A. Tahhan and F. Temurtaş, "Enhanced fuzzy logic control model and sliding mode based on field oriented control of induction motor," *World Journal of Engineering and Technology*, vol. 12, no. 01, pp. 65–79, 2024, doi: 10.4236/wjet.2024.121004.

[15] E. Esmailzadeh, G. R. Vossoughi, and A. Goodarzi, "Dynamic modelling and analysis of a four motorized wheels electric vehicle," *Vehicle System Dynamics*, vol. 35, no. 3, pp. 163–194, Mar. 2001, doi: 10.1076/vesd.35.3.163.2047.

[16] M. Khalfaoui, K. Hartani, A. Merah, and N. Aouadj, "Development of shared steering torque system of electric vehicles in presence of driver behaviour estimation," *International Journal of Vehicle Autonomous Systems*, vol. 14, no. 1, p. 18, 2018, doi: 10.1504/IJVAS.2018.093100.

[17] T. D. Gillespie, *Fundamentals of vehicle dynamics in vehicle handling dynamic,* Society of Automotive Engineers, Pennsylvania, USA, 2021.

[18] J. Y. Wong, "Handling characteristics of road vehicles," in *Theory of Ground Vehicles*, New Jersey, USA: John Wiley & Son, Fourth, Hoboken, 2022, pp. 1135–1155. doi: 10.1002/9781119719984.ch5.

[19] M. Bensaid, B. Rached, M. Elharoussi, and A. Ba-Razzouk, "Multi-drive electric vehicle system control using backstepping strategy," *2020 1st International Conference on Innovative Research in Applied Science, Engineering and Technology, IRASET 2020*, 2020, doi: 10.1109/IRASET48871.2020.9092164.

[20] N. M. Max, N. Y. J. Maurice, E. Samuel, M. C. Jordan, A. Biboum, and B. Laurent, "DTC with fuzzy logic for multi-machine systems: traction applications," *International Journal of Power Electronics and Drive Systems (IJPEDS)*, vol. 12, no. 4, p. 2044, Dec. 2021, doi: 10.11591/ijpeds.v12.i4.pp2044-2058.

[21] H. Kada, B. Mohamed, and M. Yahia, "New anti-skid control for electric vehicle using behavior model control based on energetic macroscopic representation," *Journal of Electrical Engineering*, vol. 59, no. 5, pp. 225–233, 2008.

[22] K. Hartani, M. Khalfaoui, A. Merah, and N. Aouadj, "A robust wheel slip control design with radius dynamics observer for EV," *SAE International Journal of Vehicle Dynamics, Stability, and NVH*, vol. 2, no. 2, pp. 10-02-02–0009, Jun. 2018, doi: 10.4271/10-02-02-0009.

[23] R. Rajamani, *Vehicle dynamics and control*. Boston: Springer, 2006. doi: 10.1007/0-387-28823-6.

[24] G. Banda and S. G. Kolli, "Comparison of ANN- and GA-based DTCecar," *Journal of Power Electronics*, vol. 21, no. 9, pp. 1333–1342, Sep. 2021, doi: 10.1007/s43236-021-00273-1.

[25] A. Nasri, B. Gasbaoui, and B. M. Fayssal, "Sliding mode control for four wheels electric vehicle drive," *Procedia Technology*, vol. 22, pp. 518–526, 2016, doi: 10.1016/j.protcy.2016.01.111.

[26] J. El-bakkouri, H. Ouadi, and A. Saad, "Adaptive neuro fuzzy inference system based controller for electric vehicle's hybrid abs braking," *IFAC-Papers OnLine*, vol. 55, no. 12, pp. 371–376, 2022, doi: 10.1016/j.ifacol.2022.07.340.

[27] N. El Ouanjli *et al.*, "Modern improvement techniques of direct torque control for induction motor drives - a review," *Protection and Control of Modern Power Systems*, vol. 4, no. 2, pp. 1–12, Apr. 2019, doi: 10.1186/s41601-019-0125-5.

[28] I. Takahashi and Y. Ohmori, "High-performance direct torque control of an induction motor," *IEEE Transactions on Industry Applications*, vol. 25, no. 2, pp. 257–264, 1989, doi: 10.1109/28.25540.

BIOGRAPHIES OF AUTHORS

Njock Batake Emmanuel Eric was born in Cameroon on November 13th, 1991. He received the Engineering degree from the National Advanced School of Engineering at the University of Yaoundé, Cameroon, in 2019, and the master's degree from the Postgraduate School for Pure and Applied Science (POSPAS) in Douala, in 2020, both in electrical engineering. He is currently working toward the Ph.D. degree at the Laboratory of Energy, Materials, Modeling, and Methods of the POSPAS, in the Department of Robotics. His research interests include modeling and modern control of electrical machines using neural and fuzzy logic control, applied to power electronics systems and electric vehicles. He can be contacted at email: e.njockbatake@gmail.com.

Nyobe Yome Jean Maurice was born in Yaoundé, Cameroon. He received the Diploma degree in Electrical Engineering from Advanced Teacher Training College for Technical Education from the University of Douala-(ATTCTE/ENSET), Cameroon, in 1984, and joined the University of Douala-ENSET as a lecturer, where he is currently an Associate Professor. He received the M.S. degree in Electrical Engineering jointly from the Ecole Normale Supérieurede Cachan, Franceand the Universitéde Paris VI, Paris, France, in 1986, and the Ph.D. degree in Electrical Engineering from the Université Monpellier II (STL), France 1993. He is a senior member of the Cameroon Commission for Technical Education. His area of interest is resonant power conversion, high-power variable-speed drives, windmill/diesel twinning, and applied pedagogical science to electrical engineering. He is actually the Deputy Director of the National Higher Polytechnic School of Douala. He can be contacted at email: nyobeyome@yahoo.fr.

Ngoma Jean Pierre was born in Pointe-Noire, Congo-Brazzaville. In 1992, he received the Diploma of Master of Science in Electrical Stations from the Vinnitsya National Technical University, Ukraine. In 1997, He obtained a Ph.D., Engineering Sciences, specialty: mathematical modeling in research (electrical engineering). In 2007, he was a lecturer and researcher at the University of Douala, Douala, Cameroon. His research interests include automation of energetic systems, modeling of energetic systems, renewable energy sources, and other thematic for the production, transfer, and distribution of electrical energy. He can be contacted at email: ngoma8273@gmail.com.

Ndoumbé Matéké Max is a lecturer and researcher at the University of Douala, Cameroon. Holder of a teacher's diploma of technical high schools' option, Electrotechnics, obtained in 2012, and a master's degree in Electrotechnics, Electronics, Automation, and Telecommunication at the University of Douala in 2015. He obtained a Ph.D. in Engineering Sciences with a specialization in Industrial Electronics and Systems. Research interests: power conversion, high-power, variable-speed drives, electric vehicles. He can be contacted at email:mdesmax@yahoo.fr.